Femtosecond carrier dynamics in implanted and highly annealed polycrystalline silicon

2006 Semicond. Sci. Technol. 21 1041

(http://iopscience.iop.org/0268-1242/21/8/010)

INSTITUTE OF PHYSICS PUBLISHING SEMICONDUCTOR SCIENCE AND TECHNOLOGY

Semicond. Sci. Technol. **21** (2006) 1041–1046 doi:10.1088/0268-1242/21/8/010

Femtosecond carrier dynamics in implanted and highly annealed polycrystalline silicon

Emmanouil Lioudakis[1], **A G Nassiopoulou**[2] **and Andreas Othonos**[1]

[1] Research Center of Ultrafast Science, Department of Physics, University of Cyprus, PO Box 20537, 1678, Nicosia, Cyprus
[2] IMEL/NCSR Demokritos, PO Box 60228, 15310, Aghia Paraskevi, Athens, Greece

E-mail: othonos@ucy.ac.cy

Received 24 February 2006, in final form 1 June 2006
Published 26 June 2006
Online at stacks.iop.org/SST/21/1041

Abstract

We have studied the ultrafast optical response of highly implanted and highly annealed polycrystalline silicon films using 400 nm ultrashort amplified pulses with fluence ranging between 8 mJ cm^{-2} to 56 mJ cm^{-2}. Transient reflection measurements reveal differences both in the short and long temporal behaviour between the implanted non-annealed and annealed samples. Important contributing factors to the dynamics of the non-annealed sample are the carrier recombination centres and traps induced by ion implantation. In contrast to the non-annealed sample, the Auger recombination process is a key factor in the dynamics in the first few picoseconds for the sample annealed at 1100 °C. A model based on two coupled differential equations has been employed to investigate in detail the carrier dynamics in these systems. Parameters including carrier trapping times, diffusion coefficients and the Auger coefficient have been extracted.

1. Introduction

Femtosecond carrier dynamics in semiconductors have been investigated using excitation-probe techniques over the past two decades [1–3]. Although a lot of research has been devoted to this area, the continuous miniaturization of semiconductor devices into the nano-scale regime and the complexity of the devices themselves have emphasized the importance of understanding carrier dynamics on an increasingly shorter timescale and over a large span of energy excitations. Clearly, the understanding of semiconductor processing such as ion implantation and subsequent annealing on the carrier dynamics is of critical importance in the microelectronics industry. The recent demand for high-speed micro-electronic devices with ultrafast response has given renewed interest in this area. Although crystalline silicon has a slow response, when it is rendered locally amorphous through ion implantation, it shows different temporal behaviour [3–5] due to the introduction of defects into the crystalline semiconductor, which act as traps and recombination centres [6]. Following optical excitation, electrons and holes undergo spatial and temporal evolution with characteristic times, which depend on the various relaxation processes [1]. Initially, the excitation energy is transferred entirely to the carriers, leading to the creation of non-equilibrium carrier densities with specific momentum states and elevated carrier temperatures. As the system evolves towards equilibrium, there is momentum and energy relaxation. Momentum relaxation occurs on a femtosecond timescale via elastic and inelastic scattering. On the same timescale carrier–carrier scattering of the electrons (holes) results in Coulomb thermalization and allows the electron (hole) system to be described by a Fermi–Dirac distribution. Similarly, electron–hole scattering eventually brings the two distributions into thermal equilibrium. Eventually energy relaxation of these carriers results in transferring energy to the lattice. The dynamics of these photo-generated carriers can be monitored directly using time resolved reflectivity measurements [1, 2]. Although there has been considerable research using pump-probe techniques in crystalline silicon, there is a lack of work in probing polycrystalline silicon

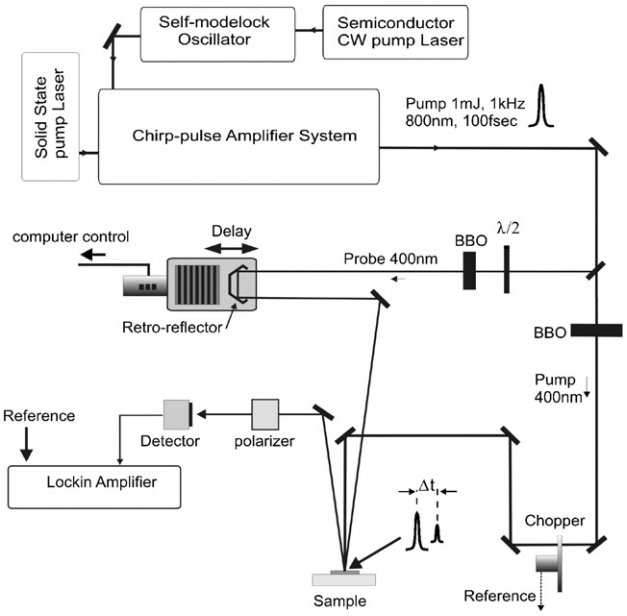

Figure 1. The above schematic shows the experimental set-up utilized in obtaining ultrafast transient reflectivity measurements.

at high fluence excitation. Here we report on ultrafast transient reflectivity measurements using highly implanted and annealed polycrystalline silicon in order to obtain a better understanding of the carrier dynamics at high excitation.

2. Experiment

In this work the temporal behaviour of reflectivity is investigated using an ultrafast femtosecond laser source. The source consists of a self mode-locked Ti:Sapphire oscillator generating 100 fs pulses at 800 nm. A regenerative amplifier system is used to amplify the pulses to approximately 1 mJ at a repetition rate of 1 kHz. The ultrashort pulses are used in a pump probe set-up (see figure 1) where the pump beam is frequency doubled at 400 nm using a nonlinear crystal (BBO). A half wave plate and a polarizer in front of the BBO crystal were utilized to control the intensity of the pump incident on the sample. A small part of the fundamental energy was also used to generate 400 nm by focusing the beam on a second BBO crystal. The 400 nm probe light which is perpendicularly polarized to the pump beam is used in a non-collinear geometry, in a pump-probe configuration. The reflected beam is directed onto a silicon detector after passing through a polarizer rejecting the scattered light from the pump beam. The differential reflected signal was measured using a lock-in amplifier with reference to the optical chopper frequency of the pump beam. The temporal variation in the index of refraction was monitored as a change in the reflectivity, which was a direct measure of the photo-excited carrier dynamics within the probing region. In this work optical pumping at a fluence up to an accumulating optical damage threshold has been used to excite the implanted polycrystalline silicon and determine its temporal behaviour. Observations of the short- and long-time behaviour in these samples have been investigated.

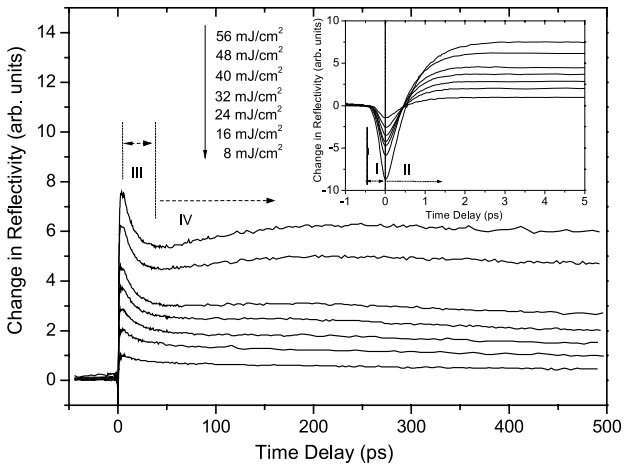

Figure 2. Transient reflectivity responses of the ion-implanted, non-annealed polycrystalline silicon sample, pumped with different excitation fluence. The inset shows the change in reflectivity at short timescales.

The samples used in these experiments were 1 μm polycrystalline silicon films on quartz implanted with arsenic ions at doses of 2×10^{16} ions cm^{-2} and implantation energy $E = 100$ keV at room temperature. After implantation, the thin oxide layer was removed and samples were then thermally annealed in a conventional furnace at 1100 °C for 1 h in an inert nitrogen atmosphere. From spectroscopic ellipsometry measurements carried out on these samples [7] it was possible to estimate the optical absorption coefficient for the implanted, non-annealed sample to be $\sim 3.5 \times 10^5$ cm^{-1} and for the sample annealed at 1100 °C 1.25×10^5 cm^{-1} at the excitation/probing wavelength.

3. Results and discussion

Figure 2 shows transient reflectivity data taken for the non-annealed sample, excited at energy densities ranging from 8 to 56 mJ cm^{-2} at 400 nm and probing at the same wavelength. The reflectivity data in this figure were obtained with 1.7 ps steps over a long temporal range from -50 ps to 500 ps. The inset figure shows the same reflectivity data over a range of up to 5 ps taken with 33.3 fs steps. Each of the time resolved curves may be divided into several distinct regions. On the short timescale, the reflectivity appears to have a pulse width limited decrease (region I), followed by a slightly slower rate increase (region II) mainly due to the generation and removal of the photo-generated carriers within the probing region. At approximately 500 fs from $t = 0$, the change in reflectivity becomes positive, reaching its maximum value at approximately $t = 4$ ps.

Following this maximum, the reflectivity begins to drop (region III) at a relatively fast rate reaching a minimum within 50 ps. At this minimum a much slower change appears to occur over hundreds of picoseconds. It is interesting to note the different long-time reflectivity behaviour of the sample when exposed at the highest excitation fluences.

The sample annealed at 1100 °C exhibits, as expected, a different behaviour both in the short and long timescales as

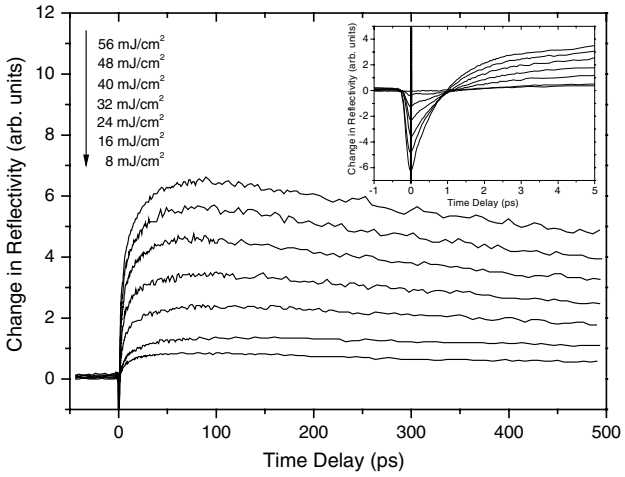

Figure 3. Transient reflectivity responses of ion-implanted polycrystalline silicon annealed at 1100 °C pumped and probed at 400 nm with various excitation fluences. The inset shows the reflectivity response on a short timescale.

seen in figure 3. Initially the ultrafast pulse excitation results in a negative change in reflectivity which is pulse width limited. Following the maximum negative change, there is recovery of the reflectivity within the first picosecond (see the inset of figure 3) which is clearly slower than the corresponding change observed in the non-annealed sample. The change in reflectivity eventually becomes positive with its maximum value being reached approximately at 90 ps. Following this maximum, the reflectivity slowly returns towards equilibrium due to thermal diffusion where the lattice temperature returns to its ambient value.

The observed changes in the reflectivity may be attributed to changes in the dielectric function associated with the presence of free-carriers and changes in the dielectric function associated with interband transitions. The free carrier contribution is commonly described with the Drude model. The interband contribution can arise from lattice temperature changes, state filling and band-gap renormalization. Both the carrier density and lattice temperature are coupled to reflectivity through the complex index of refraction where the change in reflectivity may be written in the following simple form;

$$\frac{\Delta R}{R} \approx \frac{4\Delta n[(n^2-1)-\kappa^2]+8n\kappa\Delta\kappa}{[(n+1)^2+\kappa^2][(n+1)^2+\kappa^2]}, \tag{1}$$

where Δn is the pump laser induced change in the index of refraction which may be estimated from the sum of the carrier ($\Delta n_{\Delta N}$) and temperature ($\Delta n_{\Delta T}$) contributions. Similarly $\Delta\kappa$ is the laser induced change of the extinction coefficient. Region I for both samples corresponds to a negative change in the reflectivity due to the photo-generated carriers following the ultrafast pulse excitation at 400 nm. Given the dynamics in a semiconductor following short pulse excitation, the only non-negligible contribution to the change in the reflectivity on a 100 fs timescale is the carrier density contribution. Using the dielectric function from the classical Drude model we may estimate the index of refraction and extinction coefficient changes due to the carrier density changes using the following expressions:

$$\Delta n_N = -\frac{e^2N}{2\varepsilon_0 m^*\omega^2}\left(\frac{n}{n^2+\kappa^2}\right),$$
$$\Delta\kappa_N = \frac{e^2N}{2\varepsilon_0 m^*\omega^2}\left(\frac{\kappa}{n^2+\kappa^2}\right), \tag{2}$$

where N is the carrier density, e is the charge of the carriers, m^* is the effective mass, ε_0 is the dielectric constant in vacuum and ω is the angular frequency of the excitation pulse. Under our experimental conditions the estimated change in the reflectivity following short pulse excitation is approximately 3%. This value is in a very good agreement with the measured change in reflectivity. Region II shows a fast recovery of the reflectivity associated with the removal of the carriers from the probing region. This is a combination of effects including diffusion, carrier trapping due to the centres generated by ion implantation, surface recombination and Auger recombination. For the non-annealed sample the recovery of the reflectivity signal on the short timescale is predominately due to the reduction in excited carrier density mainly from the ion-induced defects which act as recombination centres and carrier diffusion. The energy absorbed by the lattice due to energy relaxation of the hot carriers can produce a large contribution to the change in reflectivity, as clearly seen in figure 2, as a positive rise in the negative change observed on the short timescale.

Region III of the ion-implanted, non-annealed sample exhibits a decay at approximately $t = 4$ ps. The decay values range between 25 ps for the lowest fluence and 15 ps for the highest fluence. What is important to note is that the decay depth has a linear dependence within the range of fluence used in this experiment. It is our belief that this behaviour is due to the release of carriers captured earlier by traps in the ion-implanted sample. These carriers are released within the probing region causing a free-carrier negative contribution to the reflectivity.

Exposure at high fluence of the implanted and non-annealed sample causes permanent change in reflectivity which may be due to damage of the sample. This was supported from measurements taken at low fluences before and after exposure of the sample at high fluences which reveal permanent changes in reflectivity. Permanent change in the reflectivity is not evident when the sample is exposed to fluences lower than 70 mJ cm^{-2}.

Figure 4 shows the peak changes in reflectivity following the ultrashort pulse excitation for the implanted non-annealed and annealed sample at 1100 °C. The induced negative change in reflectivity which is attributed to the carriers generated within the probing region reveals a non-trivial dependence on the pump intensity. The non-annealed sample initially exhibits a near linear response as a function of pump-fluence as expected from the Drude contribution to the change of the index of refraction. Saturation effects appear at the high fluence which may be due to Auger recombination, as expected at the high carrier densities.

The change in the peak reflectivity of the annealed sample appears to have a square dependence on the fluence, as

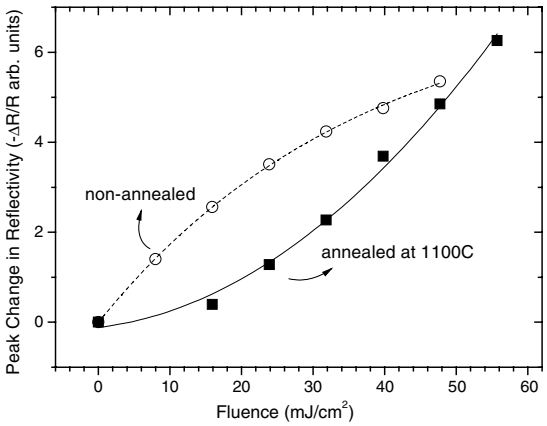

Figure 4. Peak change in reflectivity of the non-annealed (open circles) and annealed sample at 1100 °C (solid squares). The line through the solid squares is a quadratic fit to the experimental data whereas the line through the open circles is a guide to the eye.

shown by the fitted curve in figure 4. This is a strong indication of a two photon absorption process in this sample.

3.1. Carrier density and a lattice temperature model

To describe the carrier dynamics in more detail we make use of a model based on two coupled differential equations, one for the carrier density and the other for the lattice temperature. These equations include diffusion and recombination of carriers. The boundary conditions used in this model correspond to the front and back surfaces of the sample. The simple differential equation of the carrier density along with the initial and boundary conditions are

$$\begin{aligned} &\frac{\partial N(z,t)}{\partial t} = D_N \frac{\partial^2 N}{\partial z^2} - \frac{N}{\tau_R}, && N(z,0) = N_0 \exp(-\alpha z), \\ &\left.\frac{\partial N}{\partial z}\right|_{z=0} = \frac{S}{D_N} N(0,t), && N(\infty,t) = 0. \end{aligned} \tag{3}$$

Here N corresponds to the carrier density, D_N is the ambipolar diffusion coefficient, τ_R is the carrier recombination time, corresponding to the trapping time (this is the time required for the carriers to be captured by the traps). S represents the surface recombination. Similarly the differential equation for the lattice temperature and its associate initial and boundary conditions are

$$\begin{aligned} &\frac{\partial \Delta T(z,t)}{\partial t} = D_L \frac{\partial^2 \Delta T}{\partial z^2} + \frac{E_g}{\rho C} \frac{N}{\tau_{e\text{-}h}}, \\ &\Delta T(z,0) = \Delta T_0 \exp(-\alpha z), \\ &\left.\frac{\partial \Delta T}{\partial z}\right|_{z=0} = -\frac{E_g}{\rho C} \frac{S}{D_N} N(0,t), \qquad \Delta T(\infty,t) = 0, \end{aligned} \tag{4}$$

where D_L is the thermal diffusivity, E_g the band gap energy, $\tau_{\text{e-h}}$ is the electron–hole recombination time and ρ the density of the material.

The above set of equations may be solved analytically as described in [8, 9]. The solution carrier density diffusion equation is given by the following expression:

$$\begin{aligned} N(z,t) = {} & \frac{N_0}{2} \exp\left[-\frac{t}{\tau_R} - \frac{z^2}{4 D_N t}\right] \\ & \times \left\{ W\left(\alpha\sqrt{D_N t} - \frac{z}{2\sqrt{D_N t}}\right) + W\left(\alpha\sqrt{D_N t} + \frac{z}{2\sqrt{D_N t}}\right) \right. \\ & - \frac{2S/D_N}{(S/D_N) - \alpha} \left[W\left(\alpha\sqrt{D_N t} - \frac{z}{2\sqrt{D_N t}}\right) \right. \\ & \left. \left. - W\left(\alpha\sqrt{D_N t} - \frac{z}{2\sqrt{D_N t}}\right) \right] \right\}, \end{aligned} \tag{5}$$

where $W(x) = \exp[x^2]erfc(x)$.

A similar solution exists for the lattice temperature. Given that the index of refraction is dependent on the carrier density and lattice temperature the induced change in reflectivity may be estimated using a simple combination of the Drude model and thermal contribution [10]. Here we should point out that due to the high carrier densities generated in this work effects such as band-filling and band gap shrinkage may have a contribution to the change in reflectivity. Following Sokolowksi–Tinten and von der Linde [13], a simple estimate of the band filling and band gap renormalization may be obtained. For the carrier densities in this work the negative Drude contribution is a factor of ten times larger than the positive band filling contribution to the change in reflectivity. Band gap renormalization is a cubic root density dependent term [14] and has a negative contribution to the change in reflectivity. It is estimated to be approximately five times smaller than the Drude contribution. Therefore, to a first approximation, we have included only the simple Drude model for the reflectivity change. In spite of this simple approximation using the experimental parameters of this work we have been able to obtain relatively good fits to our experimental data. It should be pointed out that Auger recombination is considered negligible for the implanted, non-annealed sample where traps formed due to implantation remove the carriers. On the other hand, for the annealed sample Auger recombination is important on the first few picoseconds. Therefore, Auger recombination was used in the model for the initial short timescale followed by carrier trapping time on the long timescale. This is incorporated in the model through the carrier recombination time constant τ_R.

3.2. Simulations for a non-annealed sample

The observed transient reflectivity for the implanted sample has an added feature marked in figure 2 as region III. In this temporal region between 4 ps to 50 ps from the $t = 0$ carriers initially captured by traps are released within the probing region causing a negative free-carrier contribution to the change in the reflectivity. In the above two coupled differential equations model we have incorporated a third equation (similar to the carrier density differential equation 3) describing the generation of the released carriers into the lattice following the maximum change in reflectivity. The characteristic carrier lifetime for this equation is given by τ_l and corresponds to the carrier-trapping lifetime.

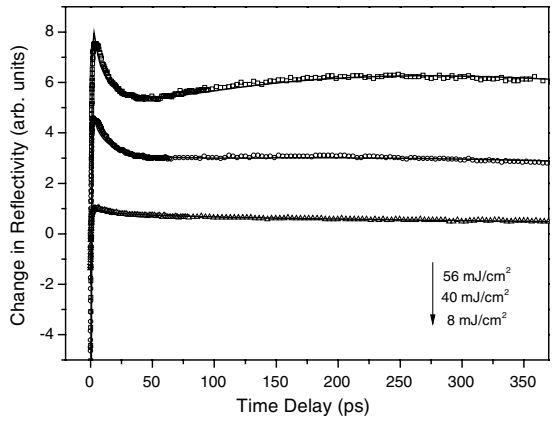

Figure 5. Fits to the experimental data for the implanted sample for fluences at 8, 40 and 56 mJ cm^{-2} using the coupled differential equations model.

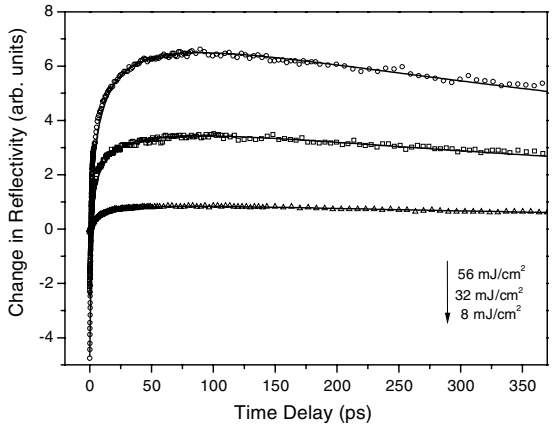

Figure 6. Fits to the experimental data for the implanted and annealed at 1100 °C sample for fluences at 56, 32 and 8 mJ cm^{-2} using the coupled differential equations of the above model.

Parameters that were varied and optimized for the best-fit results were ambipolar diffusion coefficient, carrier trapping time, electron–hole recombination and trapping carrier lifetime. All other parameters were assumed close to the values of silicon, $\rho = 2.33$ g cm^{-3}, $E_g = 1.14$ eV, specific heat $C = 0.7$ J gK^{-1} [11]. Parameters such as the surface recombination 2×10^3 cm s^{-1}, an index of refraction 5.2 and the extinction coefficient 0.9 were obtained from photo-thermal and optical measurements performed on these samples. Figure 5 shows the best fits to the experimental data for fluence at 8 mJ cm^{-2}, 40 mJ cm^{-2} and 56 mJ cm^{-2} corresponding to carrier densities of 1.1×10^{21} cm^{-3} to 7.8×10^{21} cm^{-3}. In all cases the carrier trapping time τ_R was determined to be approximately 0.54 ps and the diffusion coefficient 0.1 cm^2 s^{-1}. The fitted τ_l was determined to be between 20–15 ps.

3.3. Simulations for an annealed sample

Figure 6 shows the best fits obtained using the model based on two coupled differential equations corresponding to the fluence of 8 mJ cm^{-2}, 32 mJ cm^{-2} and 56 mJ cm^{-2}. In all these simulations the carrier trapping time τ_R was determined to be 100 ps, and diffusion coefficient 10 cm^2 s^{-1}.

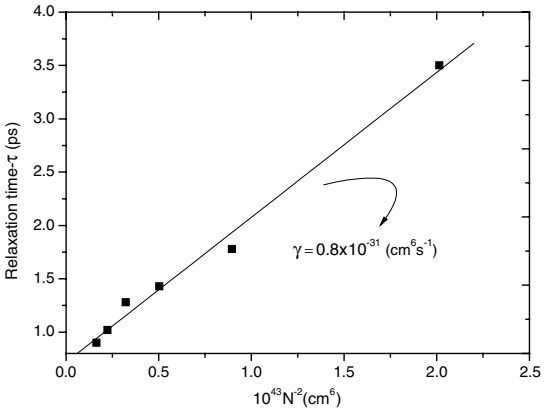

Figure 7. Auger recombination measured for the annealed sample at 1100 °C (solid squares). The line through the solid squares is a linear fit to the experimental data giving an Auger recombination coefficient of 0.8×10^{-31} cm^6 s^{-1}.

Simulations of the temporal reflectivity on the short timescale seen in the inset of figure 3 for this material using the above model allowed the extraction of the Auger relaxation time. The time constant of Auger recombination may be estimated from the expression [12]

$$\tau_A = \gamma^{-1} N^{-2}, \tag{6}$$

where γ is the Auger recombination coefficient and N is the carrier density. Figure 7 shows a plot of the relaxation time as a function of the inverse square of the carrier density. From the linear fit shown in this figure the Auger recombination coefficient was estimated to be 0.8×10^{-31} cm^6 s^{-1}. This value is in good agreement with the known Auger coefficient values for silicon.

4. Conclusions

We have investigated ultrafast carrier dynamics in ion implanted and annealed polycrystalline silicon films. The recombination centres in the implanted sample play an important role in both long- and short-time behaviour of the carrier dynamics and energy relaxation. In the sample annealed at 1100 °C after ion implantation, two-photon absorption is a key process for generating carriers, whereas Auger recombination is the dominating process of relaxation in the short timescale in this material. A two coupled differential equations model corresponding to carrier density and lattice temperature has be utilized to fit the experimental data. The extracted results suggest short carrier trapping time for the implanted non-annealed sample and small diffusion coefficient. On the other hand, for the annealed sample, fitting results suggest long carrier trapping time and a diffusion coefficient close to that of crystalline silicon.

References

[1] Shah J 1999 *Ultrafast Spectroscopy of Semiconductors and Semiconductor Nanostructures* (Berlin: Springer)
[2] Othonos A 1998 *Appl. Phys. Rev.* **83** 1789

[3] Sabbah A J and Riffe D M 2002 *Phys. Rev.* B **66** 165217
[4] Kuhl J, Göbel E O, Pfeiffer Th and Jonietz A 1984 *Appl. Phys.* A **34** 105
[5] Wright O B, Zammit U, Marinelli M and Gusev V E 1996 *Appl. Phys. Lett.* **69** 553
[6] Doany F E, Grischkowsky D and Chi C C 1987 *Appl. Phys. Lett.* **50** 460
[7] Lioudakis E, Nassiopoulou A G and Othonos A 2006 *Thin Solid Films* **496** 253
[8] Takayuki Tanaka, Akira Harata and Tsuguo Sawada 1997 *J. Appl. Phys.* **82** 4033
[9] Hoffman C A, Jarasiunas K, Gerritsen H J and Narmikko A V 1978 *Appl. Phys. Lett.* **33** 536
[10] Othonos A and Christofides C 2002 *Phys. Rev.* B **66** 085206
[11] Landolt-Bornstein 1982 *Numerical Data and Functional Relationships in Science and Technolgy* vol 17 ed O Madeling, M Schult and H Weisst (New York: Springer)
[12] Yoffa Ellen J 1980 *Phys. Rev.* B **21** 2415
[13] Sokolowksi-Tinten and von der Linde D 2000 *Phys. Rev.* B **61** 2643
[14] Wagner J and Del Alamo J A 1988 *J. Appl. Phys.* **63** 425